2′-Deoxyribonolactone Lesion in DNA: Refined Solution Structure Determined by Nuclear Magnetic Resonance and Molecular Modeling†

Muriel Jourdan, Julian Garcia,* Eric Defrancq, Mitsuharu Kotera, and Jean Lhomme

LEDSS, Chimie Bioorganique, UMR CNRS 5616, Université Joseph Fourier, BP 53, 38041 Grenoble Cedex 9, France

Received November 18, 1998; Revised Manuscript Received February 4, 1999

ABSTRACT: The solution conformation of the DNA duplex d($C_1G_2C_3A_4C_5L_6C_7A_8C_9G_{10}C_{11}$)·d($G_{12}C_{13}G_{14}T_{15}$-$G_{16}T_{17}G_{18}T_{19}G_{20}C_{21}G_{22}$) containing the 2′-deoxyribonolactone lesion (L_6) in the middle of the sequence has been investigated by NMR spectroscopy and restrained molecular dynamics calculations. Interproton distances have been obtained by complete relaxation matrix analysis of the NOESY cross-peak intensities. These distances, along with torsion angles for sugar rings and additional data derived from canonical A- and B-DNA, have been used for structure refinement by restrained molecular dynamics (rMD). Six rMD simulations have been carried out starting from both regular A- and B-DNA forms. The pairwise rms deviations calculated for each refined structure are <1 Å, indicating convergence to essentially the same geometry. The accuracy of the rMD structures has been assessed by complete relaxation matrix back-calculation. The average sixth-root residual index ($R^x = 0.052 \pm 0.003$) indicated that a good fit between experimental and calculated NOESY spectra has been achieved. Detailed analysis revealed a right-handed DNA conformation for the duplex in which both the T17 nucleotide opposite the abasic site and the lactone ring are located inside the helix. No kinking is observed for this molecule, even at the abasic site step. This structure is compared to that of the oligonucleotide with the identical sequence containing the stable tetrahydrofuran abasic site analogue that we reported previously [Coppel, Y., Berthet, N., Coulombeau, C., Coulombeau, Ce., Garcia, J., and Lhomme, J. (1997) *Biochemistry 36,* 4817−4830].

Oxidative damage to DNA has been the object of intensive investigation over the past twenty years (*1*, *2*). Base modifications as well as sugar attack lead to lesions that are most frequently repaired in the cell by specific enzymes that are able to recognize and repair the damage (*3*). Among these, loss of a nucleic base leading to an oxidized 2′-deoxyribose moiety, i.e., 2′-deoxyribonolactone (Chart 1),

Chart 1: 2′-Deoxyribonolactone Site (**1**), 2′-Deoxyribose Site (**2**) and "Tetrahydrofuran" Analogue (**3**)

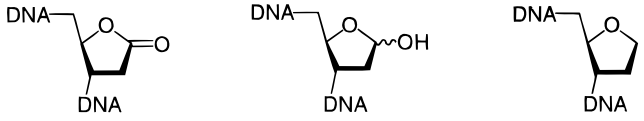

is an event that may occur under the action of quite different agents. 2′-Deoxyribonolactone has been reported to be generated due to the action of drugs, such as the ene-diyne anticancer antibiotic neocarzinostatin (*4*) and the cationic porphyrin Mn-TMPyP [manganese *meso*-tetrakis(4-*N*-methylpyridiniumyl)porphyrin] (*5*, *6*), and to γ and UV irradiation (*7*−*9*). 2′-Deoxyribonolactone has also been proposed to be formed as an intermediate in DNA cleavage by the chemical nuclease copper phenanthroline [$Cu(OP)_2$] (*10*−*13*) and by chromium(V) carcinogens (*14*). 2′-Deoxyribonolactone was also observed in the UV photoreaction of small oligonucleotides containing 5-halouracil in specific sequences (*15*). The primary event leading to 2′-deoxyribonolactone formation is considered to be hydrogen atom abstraction at the anomeric position of nucleotides by reactive radical species, the evolution of the resulting C-1′ radical differing according to the reagent involved (*16*−*18*). Elucidation of the mechanism of lactone formation is complicated due to the lability of the 2′-deoxyribonolactone fragment in DNA that is subject to successive β- and δ-eliminations, leading to strand cleavage with release of 5′- and 3′-phosphate-ending DNA fragments and recovery of 5-methylene furanone (5MF) as the main sugar residue (*12*) (Scheme 1).

Scheme 1

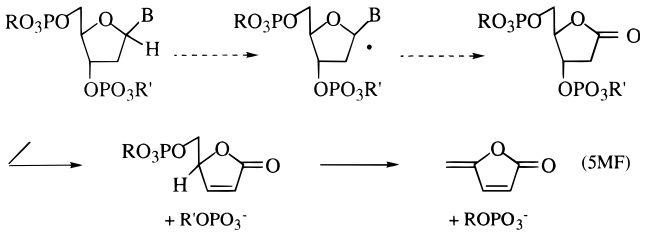

Structurally, 2′-deoxyribonolactone in DNA resembles the "regular" abasic site (AP^1 site) that results from hydrolytic cleavage of the *N*-glycosidic bond, leaving a deoxyribose residue (Chart 1), and that arises in vivo spontaneously (*19*) and as an intermediate in DNA glycosylase-mediated repair of damaged bases (*20*−*24*). However, by comparison with

† This research was supported by the Association pour la Recherche sur le Cancer (ARC), by the Ligue Nationale contre le Cancer (LA LIGUE), and by the Région Rhône-Alpes (to M.J.).

* To whom correspondence should be addressed. E-mail: julian.garcia@ujf-grenoble.fr. Telephone: 33 (0)4 76 51 45 23. Fax: 33 (0)4 76 51 43 82.

10.1021/bi982743r CCC: $18.00
Published on Web 03/11/1999

the latter 2′-deoxyribose abasic sites that are the object of numerous studies, very little is known about the fate of 2′-deoxyribonolactone damage in the cell. It has been reported that the lesion is mutagenic (*25*) and that it is recognized, although less efficiently, by those repair enzymes that are in charge of the regular abasic site lesions, such as endonuclease IV and exonuclease III (*26*−*28*). This suggests that the local conformation of DNA at regular and at oxidized abasic sites could play a crucial role in the recognition of the lesions by the AP endonucleases.

General information concerning modification in the DNA structure brought about by the presence of regular 2′-deoxyribose abasic sites has been obtained by different authors who examined synthetic DNA fragments containing either a deoxyribose unit (*29*−*32*) or, in most of the studies, the stable tetrahydrofuran analogue of the abasic site that has been demonstrated to retain the biological properties of the natural abasic site (*33*) (Chart 1). High-field NMR showed that oligonucleotides containing the abasic site opposite a purine residue, i.e., apyrimidinic sites, conserve a regular right-handed DNA geometry in which the base opposite the lesion and the abasic site stack inside the helix (*34*−*37*). On the other hand, oligonucleotides containing the lesion opposite a pyrimidine residue, i.e., apurinic sites, exhibit additional conformational flexibility. Both the abasic sugar residue and the opposing pyrimidine are intrahelical (*35*, *38*) and sometimes extrahelical (*35*). No comparable information is available concerning the 2′-deoxyribonolactone site.

The paucity of biological and structural data relative to 2′-deoxyribonolactone damage is largely due to the absence of a general and efficient synthesis of DNA fragments containing the lesion at any predetermined position in the sequence. We recently reported such a synthetic process (*39*). We describe here the solution structure of the duplex d($C_1G_2C_3A_4C_5L_6C_7A_8C_9G_{10}C_{11}$)·d($G_{12}C_{13}G_{14}T_{15}G_{16}T_{17}G_{18}T_{19}G_{20}C_{21}G_{22}$) as determined by high-field NMR spectroscopy and molecular dynamics. The duplex contains the 2′-deoxyribonolactone moiety (L) in the middle of the sequence, flanked by two cytosines and opposite a thymine residue. The indicated sequence was selected for comparison purposes, as we recently described the structure of the analogous duplex containing the stable tetrahydrofuran abasic site in the same position as L_6 in the identical sequence (*38*).

MATERIALS AND METHODS

Oligonucleotide Synthesis. The 2′-deoxyribonolactone-containing undecamer was prepared as previously described (*39*). The oligomer was synthesized on a 15 μmol scale on a Milligen/Biosearch 3700 DNA synthesizer. The 2′-deoxyribonolactone-containing undecamer was purified by reverse phase HPLC on a C_{18} Nucleosil column (Macherrey-Nagel). Elution was carried out with a linear gradient of MeOH (5 to 50%) over the course of 20 min in 5 mM sodium phosphate buffer (pH 6). The pure oligonucleotide was desalted on Waters Sep-Pak cartridges by washing with deionized water and eluting with a mixture of water/acetonitrile (80/20). After evaporation to dryness, the oligomer was dissolved in the NMR buffer. The primary structure of the undecamer containing the 2′-deoxyribonolactone lesion was characterized by ESMS spectra.

Sample Preparation. Due to the great instability of the 2′-deoxyribonolactone residue, the duplex was formed by mixing equimolar amounts of each strand without annealing. The NMR spectra of the undecamer were recorded in 0.1 M NaCl and 20 mM sodium phosphate buffer solution at pH 7. The final duplex concentration was 0.67 mM. For experiments carried out in D_2O, the sample was lyophilized twice from 99.8% D_2O and redissolved in 99.96% D_2O. A 90% H_2O/10% D_2O mixture was used to obtain NMR spectra of exchangeable protons.

NMR Experiments. All NMR data sets were recorded on Varian Unity Plus 500 and Varian Unity 600 spectrometers at 10 °C. Proton spectra were referenced relative to the residual HOD resonance, which had been previously calibrated to 3-(trimethylsilyl)propionate-2,2,3,3-d_4 (TSP-d_4). Phosphorus spectra were referenced relative to trimethyl phosphate (TMP).

NOESY spectra were acquired at mixing times of 50, 80, 150, and 250 ms. For each FID, 160 transients were acquired with 4096 points over a spectral width of 6000 Hz. A total of 300 FIDs were collected. Attenuation of the residual HOD resonance was achieved by low-power presaturation during the relaxation delay and during the mixing time. In the DQF-COSY spectrum, 256 transients were used and a total of 400 FIDs were collected. TOCSY spectra were collected at mixing times of 40 and 60 ms. For each FID, 160 transients were acquired with 4096 points over a spectral width of 6000 Hz. A total of 300 FIDs were collected. A two-dimensional NOESY spectrum was recorded in 90% H_2O with a mixing time of 250 ms at 500 MHz. The first pulse was replaced by a 360_x 270_{-x} composite pulse (*40*), and the last 90° pulse was replaced by a jump and return sequence to suppress the solvent signal (*41*). The maximum excitation was adjusted to 13 ppm using a delay of 60 μs between the two read pulses at 500 MHz. For each FID, 688 transients were acquired with 4096 points over a spectral width of 10 500 Hz. A total of 300 FIDs were collected.

The ^{1}H−^{31}P HSQC-TOCSY spectrum was recorded using a mixing time of 60 ms. For each FID, 2048 transients were acquired with 4096 points over a spectral width of 3500 Hz for the ^{1}H dimension and 600 Hz for the ^{31}P dimension. A total of 40 FIDs were collected.

Longitudinal relaxation times (T_1) were determined by the inversion−recovery method.

Generation of Dihedral Angles and Distance Restraints. For dihedral angle restraints, a qualitative approach for determining sugar puckers was adopted according to a procedure used in a previous study (*38*). Thus, we evaluated the cross-peak intensities from DQF-COSY by comparison with an internal standard (e.g., cytosine H5−H6) and deduced approximate values of J coupling constants (*42*). The pseudorotation angles P were then estimated through analysis of coupling constants along with close inspection of NOE intensities involving sugar protons. For all nucleosides except L_6, the P values were converted into five individual sugar torsion angles υ_j using the relationship $\upsilon_j = \psi_m \cos[P +$

[1] Abbreviations: AP, apurinic and apyrimidinic; δ, chemical shift in parts per million; NOE, nuclear Overhauser effect; NOESY, two-dimensional nuclear Overhauser effect spectroscopy; DQF-COSY, double-quantum-filtered correlation spectroscopy; TOCSY, total homonuclear correlated spectroscopy; rmsd, root-mean-square deviation; rMD, restrained molecular dynamic; ESMS, electron spray mass spectrometry.

144($j - 2$)], where $\psi_m = 38°$ and $j = 0-4$ (*43*). These torsion angles were also used for the subsequent rMD refinement.

Interproton distances entailing solely nonexchangeable protons were calculated from the NOESY cross-peak intensities at three mixing times (50, 80, and 150 ms) using the iterative complete relaxation matrix algorithm MARDIGRAS (*44*−*46*). Standard B-DNA and A-DNA (*47*) were used as starting structures, and calculations were performed using three correlation times ($\tau_c = 3$, 4, and 5 ns) assuming isotropic tumbling motion for the molecule. These correlation times were estimated by measuring the initial buildup rate for several H6−H5 vectors as indicated by Reid et al. (*48*). A three-state jump model was used to account for the internal motion of the methyl protons (*46*).

Structural Calculations. Initial starting structures were generated using the Biopolymer module of the Biosym Insight II software (*49*). The d($C_1G_2C_3A_4C_5A_6C_7A_8C_9G_{10}C_{11}$)·d($G_{12}C_{13}G_{14}T_{15}G_{16}T_{17}G_{18}T_{19}G_{20}C_{21}G_{22}$) duplex was first constructed in canonical A- and B-forms. Then, the A_6 base residue was removed and its sugar replaced by 2′-deoxyribonolactone. Sodium counterions were placed at the bifurcating positions of the O−P−O angles at a distance of 5 Å to neutralize the phosphate groups. These unminimized structures were designated as Ini-A and Ini-B.

The restrained molecular dynamic procedure (rMD) and energy minimization calculations were performed using DISCOVER version 2.97 with the AMBER force field potentials (*50*). NOE and dihedral restraining functions used were standard square-well effective potentials. A distance-dependent dielectric function $\epsilon = 4r$ was used to account for solvent effects.

The distances obtained from the MARDIGRAS calculations and the sugar ring dihedrals were incorporated into a rMD procedure with force constants of 30 kcal mol^{-1} Å^{-2} and 25 kcal mol^{-1} rad^{-2}, respectively. According to the literature (*51*), 28 distances were also included with a force constant of 25 kcal mol^{-1} Å^{-2} to enforce Watson−Crick hydrogen bonding throughout the calculations. Additionally, hydrogen bond angles were constrained to 170−190° with force constants of 25 kcal mol^{-1} rad^{-2} for all base pairs. Finally, backbone torsion angle restraints permitting a broad range of torsion space were employed for all residues but the lactone, with a force constant value of 5 kcal mol^{-1} rad^{-2}. These allowed maintenance of the right-handed character of DNA and prevention of artifacts during molecular dynamics calculations (*52*). Distance and dihedral angle restraints were applied to canonical forms Ini-A and Ini-B, which were subjected to 2000 steps of energy minimization. This was followed by simulated annealing rMD for 112 ps in the same way as described earlier (*38*). The last 10 coordinate sets of the final 10 ps were averaged and energy minimized with restraints to remove averaging artifacts. However, after the rMD procedure, some artifacts in the lactone region were present, as previously observed for the AP site-containing duplex (*38*). These are abnormally short distances in the lactone region, which led us to add "non-NOE constraints" (*53*, *54*), imposing a minimal distance of 4.5 Å for these unusually close protons.

The distance restraints were refined using the complete relaxation matrix approach (*55*, *56*). Resulting structures from rMD calculations for Ini-A and Ini-B were taken as input data for the CORMA program. Theoretical NOESY spectra were back-calculated with overall correlation times of 5 ns and compared to the experimental NOESY spectra (50, 80, and 150 ms). The "crystallographic" R^c factor and R^x factor (*57*) were used to measure the fit between experimental and calculated intensities. To minimize the difference between calculated and experimental NOESY spectra, distances were refined. Then, the rMD protocol was executed again with the new distances. These were refined again using the CORMA program, and this iterative process was repeated until the decrease of R factors leveled off.

Calculations including the refined restraints were carried out from the two Ini-A and Ini-B structures with three different initial velocity seeds for each. This yielded six restrained structures (RS-A1, RS-A2, RS-A3, RS-B1, RS-B2, and RS-B3) that were averaged to generate the final structure RS-ave. As partial fraying occurred for terminal base pairs, rmsd values were calculated only for the nine inner base pairs of each rMD structure.

Structural Analysis. Analysis of the conformational and helical parameters was carried out with the program CURVES, version 5.1 (*58*), which is especially suited for the characterization of regular or irregular nucleic acids (*59*, *60*).

RESULTS

Nonexchangeable Proton Assignments. The nucleic acid base and sugar protons were assigned on the basis of an analysis of through-space nuclear Overhauser effect (NOESY) and through-bond correlated (COSY and TOCSY) spectra using standard methods (*61*−*63*). The assigned resonances are given in Table 1. The 250 ms NOESY spectrum was used to establish sequential connectivities from the base proton to its own and 5′-flanking sugar protons. This allowed assignment of the base protons H8, H6, and H5 and of the H1′, H2′, and H2″ sugar protons. The expanded 250 ms NOESY spectrum which displayed connectivities correlating H8/H6 to H2′/H2″ is shown in Figure 1. For illustration purposes, the sequential NOE connectivities have been traced along the duplex from A_4 to A_8 on the modified strand (Figure 1A) and from T_{15} to T_{19} on the complementary strand (Figure 1B). Obviously, the interruption in the tracing at the $C_{5p}L_{6p}C_7$ step is due to the absence of base at the L_6 site. It is worth noting that medium NOEs were observed between the C_7-H6 and L_6-H2′/H2″ protons (Figure 1A). On the complementary strand, several NOEs were noticed between G_{18}-T_{17} and between T_{17}-G_{16}, which were consistent with T_{17} stacking inside the duplex. Moreover, analysis of the resonance line widths corresponding to T_{17} and L_6 revealed that these two residues were not in equilibrium with an extrahelical conformer, even at 30 °C, as reported for the d(CGTGXGTGC)·d(GCACTCACG) sequence (X is tetrahydrofuran) (*35*).

The attribution of the H1′, H2′, and H2″ resonances was further confirmed by analysis of the DQF-COSY spectrum and the other sugar protons were assigned using a combination of NOESY, DQF-COSY, and TOCSY spectra. The adenine H2 protons were easily distinguished from the other base protons in a one-dimensional inversion−recovery experiment due to their long longitudinal relaxation time. They were assigned by observing NOEs with their own and 3′-flanking anomeric protons.

Table 1: ^{1}H and ^{31}P Chemical Shift Assignments for the Duplex Containing the 2′-Deoxyribonolactone Site[a]

residue	H8	H6	H5/Me/H2	H1′	H2′	H2″	H3′	H4′	H5′/H5″	imino[b]	amino[c]	^{31}P[d]
C_1		7.68	5.96	5.80	2.06	2.48	4.76	4.11	3.76		na	
G_2	8.01			5.96	2.77	2.77	5.03	4.40	4.12	13.12		−3.80
C_3		7.43	5.51	5.68	2.10	2.44	4.90	4.24	4.19		8.46/6.62	−3.73
A_4	8.28		7.85	6.25	2.70	2.91	5.06	4.46	4.20/4.14[e]			−3.74
C_5		7.33	5.30	5.95	2.17	2.17	4.84	4.43	4.13		8.10/6.63	−3.95
L_6					2.95	2.66	4.89	4.23	3.99			−2.88
C_7		7.66	6.01	5.67	2.06	2.46	4.88	4.23	4.09		8.38/7.10	−4.25
A_8	8.36		7.83	6.21	2.79	2.91	5.06	4.46	4.17/4.06[e]			−3.80
C_9		7.29	5.36	5.63	1.96	2.34	4.83	4.16	na		8.28/6.70	−3.95
G_{10}	7.91			5.99	2.65	2.78	4.83	4.39	4.15/4.08[e]	13.16		−3.72
C_{11}		7.47	5.49	6.22	2.22	2.22	4.55	4.20	4.05		na	−3.72
G_{12}	8.01			6.05	2.69	2.84	4.91	4.29	3.76	13.10[g]		
C_{13}		7.47	5.45	5.80	2.22	2.51	4.92	4.27	na		8.52/6.67	−3.64
G_{14}	7.99			6.06	2.70	2.82	5.04	4.43	4.17	12.93		−3.91
T_{15}		7.17	1.54	5.80	1.95	2.31	4.88	4.29	4.18	13.90		−3.90
G_{16}	7.84			5.92	2.65	2.65	4.88	4.38	4.10/4.17[e]	12.83		−3.80
T_{17}		7.33	1.51	5.94	1.97	2.23	4.73	4.32	na	10.82[f]		−3.80
G_{18}	7.98			6.01	2.76	2.85	4.89	4.42	4.20/4.11[e]	12.74		−3.91
T_{19}		7.33	1.46	5.89	2.18	2.53	4.84	4.25	4.15	13.82		−4.00
G_{20}	7.94			5.92	2.68	2.73	5.01	4.41	na	12.83		−3.72
C_{21}		7.40	5.49	5.81	1.97	2.40	4.87	4.23	4.17		8.51/6.70	−3.67
G_{22}	7.99			6.21	2.66	2.39	4.72	4.24	na	13.16[g]		−3.64

[a] H_2O is referenced at 4.97 ppm. Proton assignments are at 10 °C, pH 7 (at 600 MHz), 0.1 mM NaCl, 20 mM sodium phosphate buffer, and 0.67 mM DNA. [b] Assignments of H1 imino protons of guanine and of H3 imino protons of thymine. [c] Assignments of hydrogen-bonded amino protons and exposed amino protons of cytosine. [d] ^{31}P chemical shifts are referenced to TMP at 10 °C. [e] Not differentiated. [f] Broad resonance. [g] Interchangeable. na means not assigned.

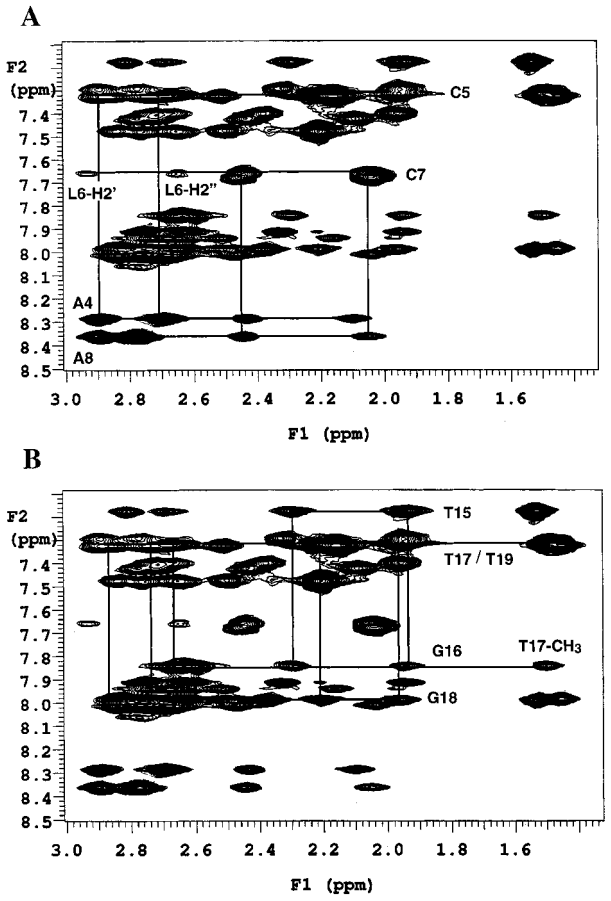

FIGURE 1: Expanded plot of the 250 ms NOESY spectrum in D_2O at 10 °C (600 MHz, 0.1 mM NaCl, 20 mM phosphate buffer, and 0.67 mM DNA) showing the correlations between aromatic and H2′ and H2″ protons. Sequential connectivities are traced from the residue A_4 to A_8 (A) and from T_{15} to T_{19} (B). Peaks corresponding to the 2′-deoxyribonolactone are labeled. Note the interruption at the L_6 step reflecting the missing base.

The protons of the 2′-deoxyribonolactone residue were assigned from the 50 ms NOESY and DQF-COSY spectra. The lactone H2′ and H2″ protons resonating at 2.95 and 2.66 ppm, respectively, were distinguished on the basis of NOE cross-peak intensities with the lactone H3′ and C_7-H6 protons.

All cross-peak intensities were consistent with predominantly S-type sugar conformation and with a right-handed helix, typical of a B-like DNA conformation.

Exchangeable Proton Assignments. The NOESY spectrum determined in H_2O showed two well-resolved thymine imino protons at 13.90 and 13.82 ppm, which were assigned to T_{15} and T_{19}, respectively. Indeed, these two resonances displayed characteristic NOE cross-peaks with the adenine H2 proton of their complementary base and with their own methyl group. Sequential connectivities between the imino protons of A·T and their adjacent C·G base pairs permitted assignment of the G_{14}, G_{16}, G_{18}, and G_{20} imino protons. Finally, NOEs between the guanine imino protons with hydrogen-bonded and exposed cytosine amino protons as well as with the nonexchangeable H5 protons confirmed these assignments, and allowed identification of the two other G_2 and G_{18} imino protons. The two terminal base imino protons were detected at 13.10 and 13.16 ppm, but were too large to be assigned due to "end fraying". The cross-peak patterns observed for the imino protons establish that all A·T and G·C base pairs are stabilized by Watson−Crick pairing throughout the duplex. The broad resonance at 10.82 ppm was assigned to the unpaired T_{17} imino proton by comparison with the AP site-containing oligonucleotide that we previously described (*38*).

Figure 2 represents the melting profile of the abasic site-containing oligonucleotide. Upon the temperature being raised to 50 °C, all the imino protons shift and broaden because of increased exchange with solvent, indicating a melting temperature between 45 and 50 °C, under the NMR conditions and DNA and salt concentrations employed. The same experiment performed on the fully paired oligonucleotide led to a melting temperature between 65 and 70 °C

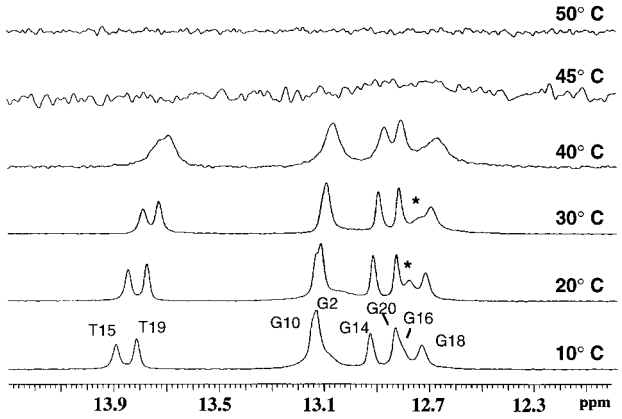

FIGURE 2: Temperature dependence of the exchangeable imino protons for the abasic duplex performed in H_2O from 10 to 50 °C (600 MHz, 0.1 mM NaCl, 20 mM phosphate buffer, and 0.67 mM DNA). The G_{16} nucleotide is labeled with an asterisk at 20 and 30 °C.

(unpublished results). A more detailed examination shows that terminal resonances first disappear, followed by the G_{16} imino resonance, which begins to broaden at about 20 °C (denoted by an asterisk in Figure 2). The latter peak and that corresponding to G_{20}-H1 are superimposed at 10 °C but well-resolved at a higher temperature. These data indicate that the C_7·G_{16} base pair, located on the 3′-side of the abasic site, is exchanging more rapidly with the solvent than with the other nonterminal base pairs. A somewhat shorter lifetime is also observed for the G_{18} imino proton when compared to the other inner guanine residues.

Phosphorus Assignments. ^{31}P resonances were assigned at 10 °C from a heteronuclear ^{31}P−^{1}H HSQC-TOCSY spectrum. Attributions are given in Table 1. Sequential assignment of the ^{31}P signal of the *i*th phosphate was achieved through connectivities with the H3′ (*i*−1), H4′ (*i*), and H5′−H5″ (*i*) protons (*64*). When the TOCSY relay is efficient, it is possible to connect the *i*th phosphate to the H2′/H2″ (*i*−1) protons.

The range of ^{31}P chemical shifts is 1.34 ppm, with one phosphate slightly shifted downfield from the region normally observed for DNA duplexes. This peak was assigned to the L_6 nucleotide (−2.88 ppm) on the basis of its correlation with both C_5-H3′ and L_6-H4′ protons. The C_7 phosphorus, and the two phosphorus atoms flanking the T_{17} residue, are less perturbed as they appear at −4.25, −3.80, and −3.91 ppm. These results indicate a distortion of the backbone limited to the abasic site step.

Sugar Puckers. From the DQF-COSY spectrum, it was rather difficult to measure precisely the coupling constants of the sugar protons due to severe overlapping and large resonance line widths. However, the magnitude of the coupling constants is known to be proportional to the cross-peak intensities observed in the DQF-COSY spectrum (*42*). Thus, we adopted a qualitative approach for determining sugar puckers. A total of 105 endocyclic torsion angle restraints (five per residue, except for L_6) were calculated. All the *P* values were in the 90−180° range, consistent with an S-type conformation. On the whole, predominant geometry was found to be C2′-endo (P = 162−180°) since 12 out of 22 nucleosides, i.e., G_2, C_5, C_7, G_{10}, C_{11}, G_{12}, C_{13}, G_{14}, T_{15}, G_{16}, G_{18}, and T_{19}, do not show detectable H3′−H4′ cross-peaks in the DQF-COSY spectrum. The C_3, A_4, A_8, C_9, G_{20}, and C_{21} residues showed strong H3′−H4′ cross-peaks with nonexistent H2″−H3′ cross-peaks characteristic of C1′-exo sugar pucker (P = 108−144°). For C_1 and G_{22}, *P* ranged from 90 to 120° with respect to strong intensities of H3′−H4′ cross-peaks and weak but detectable H2″−H3′ cross-peaks. Only T_{17} exhibited a weak H3′−H4′ cross-peak with a nonexistent H2″−H3′ cross-peak constraining *P* in the 140−162° range.

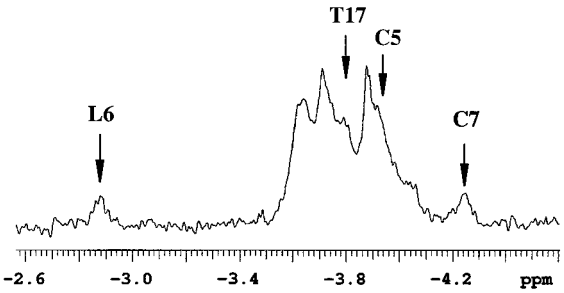

FIGURE 3: Selected resonances of the one-dimensional ^{31}P NMR spectrum (202 MHz, 10 °C, 0.1 mM NaCl, 20 mM phosphate buffer, and 0.67 mM DNA).

NOE Intensity Analysis. A total of 136, 155, and 180 NOE cross-peak intensities were measured in the 50, 80, and 150 ms NOESY spectra, respectively. These integrated cross-peaks were then used in the total relaxation matrix analysis. The distances obtained from MARDIGRAS calculations which exhibited large variations were discarded as they resulted from dramatic peak overlap or from signal-to-noise ratios that were too low. Thus, the final combined set of distances from all three NOE data sets provided 172 distance restraints. Each individual restraint was introduced in the rMD calculations with the smallest range between the upper and lower bound being imposed at 10% of the average value.

Structural Calculations. A set of six rMD calculations was performed with different random number seeds starting from either A- or B-DNA. A total of 198 experimental interproton distance restraints, 105 sugar dihedral restraints, 94 backbone torsion angles which maintain the right-handed character of the helix, and 56 restraints which preserve base pairing were used for structural calculations. Figure 4 shows the superimposition of the six refined structures (RS-A1, RS-A2, RS-A3, RS-B1, RS-B2, and RS-B3) and reveals that they all converge to essentially the same geometry. Successful convergence from different starting structures has been further confirmed by comparison of the atomic rmsd values, reported in Table 2 for the various models. The rmsd values between any one of the six rMD structures and either of the initial forms is quite large, suggesting a significant difference between refined and standard geometries.

The agreement between experimental NOE cross-peak intensities and theoretical values calculated for the rMD structures was estimated by the residual indices R^c and R^x, using the CORMA program. Table 2 shows *R* factors observed for the starting and refined structures. From these results, it appears that all rMD structures are very consistent with the experimental data, as can be seen by significant reduction in the *R* values ($R^x \leq 0.053$) when compared to those of initial Ini-A and Ini-B structures. It can thus be concluded that good accuracy in the structures has been achieved.

Structural Analysis. To gain more insight into structural details, all helical parameters, backbone torsion angles, and sugar conformations of the six rMD structures have been

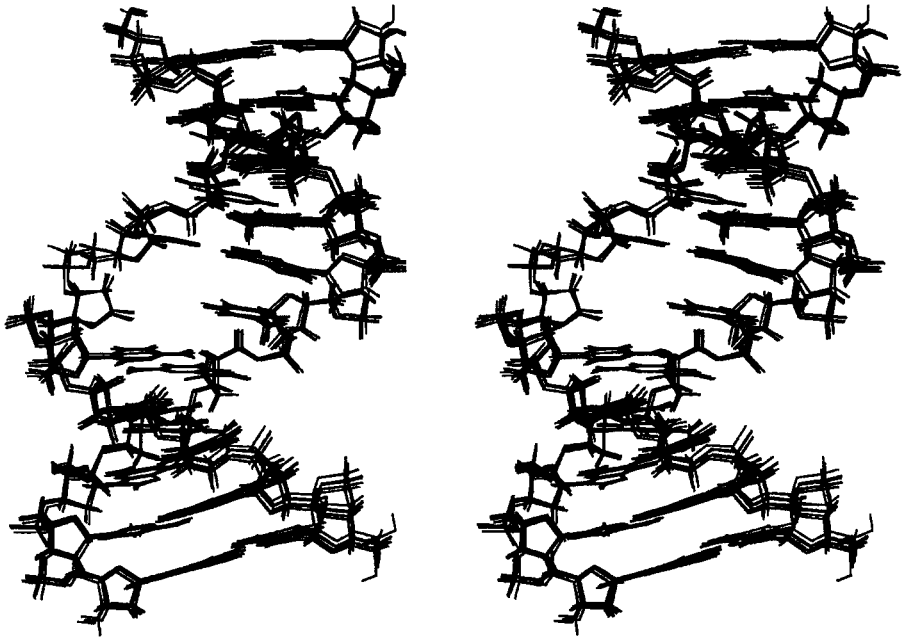

FIGURE 4: Stereoview showing the superimposition of the six refined structures viewed into the minor groove.

Table 2: Atomic rmsd Values[a] (Å) and R^c and R^x Factors[b]

	rmsd (Å)									
	Ini-B	RS-A1	RS-A2	RS-A3	RS-B1	RS-B2	RS-B3	RS-ave	R^c factor	R^x factor
Ini-A	5.20	3.07	3.21	2.92	3.34	3.25	3.17	3.07	1.00	0.188
Ini-B	***	2.81	3.13	2.95	2.42	2.54	2.66	2.73	0.70	0.110
RS-A1		***	0.18	0.31	0.97	0.95	0.88	0.63	0.21	0.052
RS-A2			***	0.44	0.93	0.94	0.89	0.67	0.22	0.052
RS-A3				***	0.98	0.95	0.93	0.65	0.21	0.053
RS-B1					***	0.14	0.37	0.65	0.22	0.053
RS-B2						***	0.33	0.61	0.21	0.052
RS-B3							***	0.55	0.21	0.052

[a] rmsd between starting structures (Ini-A and Ini-B) and refined structures (RS-A1, RS-A2, RS-A3, RS-B1, RS-B2, and RS-B3), excluding the end base pairs. [b] Crystallographic-like NMR R^c factor and sixth-root weighted NMR R^x factor of the 150 ms mixing time.

calculated with the CURVES program (*58*). Selected helix parameters and backbone angles are displayed in Figures 5 and 6, and compared with those of canonical A- and B-DNA.

(a) Backbone Torsion Angles. Values of torsion angles $\alpha-\zeta$ for the six rMD structures along with that of canonical A- and B-DNA (*47*) are presented in Figure 5A. These plots generally reveal no large fluctuation for the backbone torsion angles despite the limited number of direct experimental restraints, implying that they are further constrained by the indirect restraints and the empirical force field. The α, β, γ, and δ angles for all but the C_7 residue converge well inside the canonical range for the A- or B-DNA form. The common B_I state is observed for the phosphate backbone with an ϵ angle in the trans conformation and ζ angles in the $-$gauche boundary range.

Formation of $\alpha\gamma$ crankshafts are observed for the C_7 nucleotide. The α dihedral angles display a common $-$gauche value for three of the rMD structures and a trans conformation for the others. On the other hand, the γ angles move from a trans to a more common $+$gauche conformation. These deformations keep the length of the phosphodiester backbone approximately unchanged and maintain regular base stacking in the duplex. Such broad variations indicate that C_7 is ill-defined and that the most important structural perturbations arise at the abasic site. These perturbations seem to extend to the 3′-flanking A_8 residue which displays a relatively large distribution in its torsion angles.

No significant changes of torsion angle values occur at the T_{17} nucleotide which faces the abasic site.

(b) Glycosidic Torsion Angles and Sugar Puckers. The glycosidic torsion angles χ adopt a wide range of values between $-86°$ and $-131°$ indicative of anti conformations (Figure 5B).

The pseudorotation angles *P* agree well with the canonical B-DNA, except for terminal bases C_1 and G_{22}. For the inner base pairs and T_{17} residue, all the values are $>120°$, consistent with a predominantly S conformation of the deoxyribose moieties (Figure 5B). Terminal nucleotides C_1 and G_{22} exhibit sugar puckers intermediate between those of A- and B-DNA forms, as usually found for a solution structure of DNA.

Helical Parameters. Data summarizing the orientation of the base pairs relative to the helix axis are plotted in Figure 6A. Among the axis$-$base pair parameters, *X*-axis displacements appear to be larger than those for standard B-DNA but consistent with right-handed helix (-2 to -3.4 Å) (data not shown). Unlike canonical geometries, *Y*-Axis displacements also display non-zero but slightly positive values (data not shown). Base pair inclinations have values midway between those of canonical A- and B-DNA forms. Tip angles are similar to those of regular A- and B-DNA structures, fluctuating from $-5°$ to 4°.

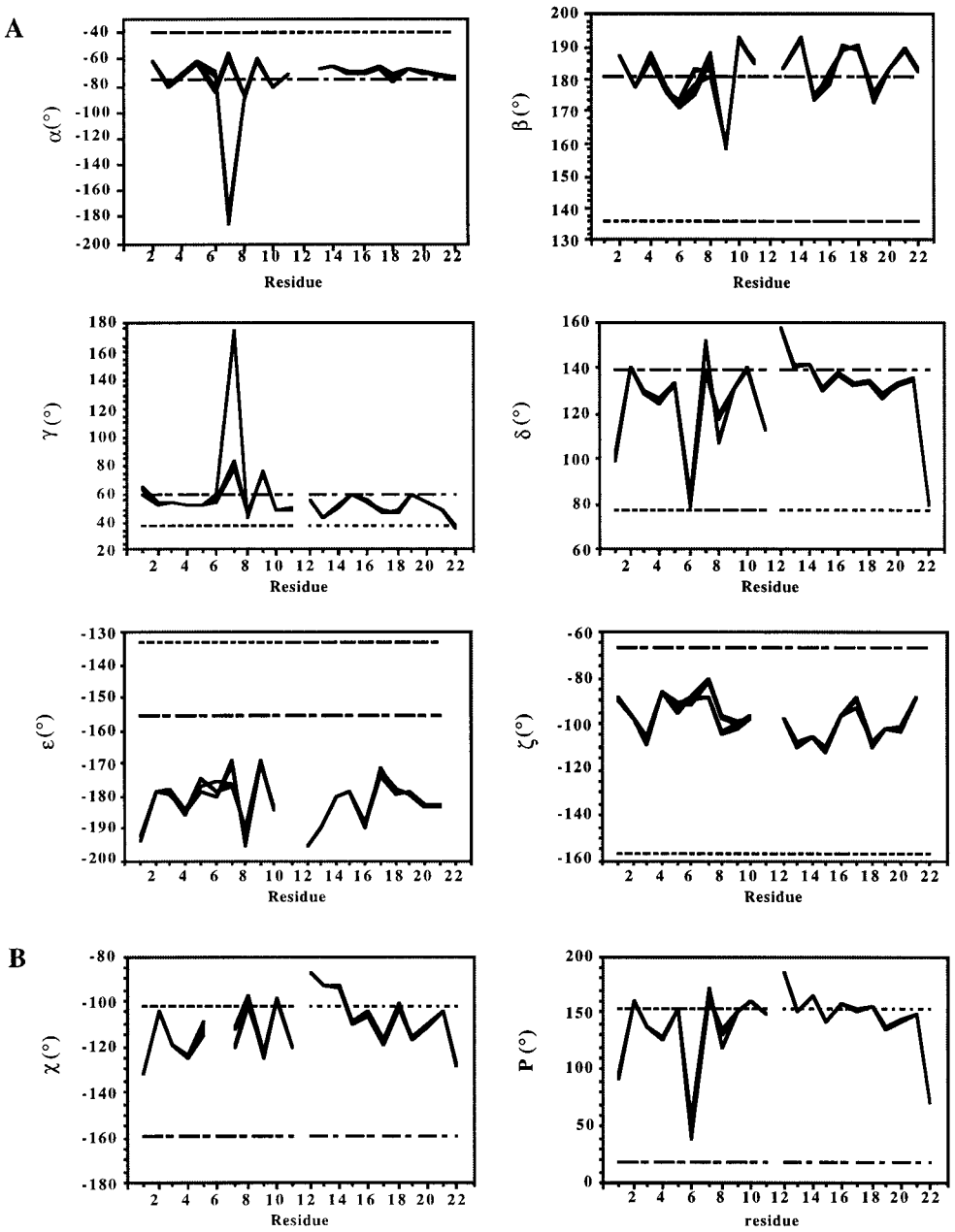

FIGURE 5: Backbone torsion angles (A) and glycosidic torsion angles and sugar pseudorotation angles (B) for the six resulting rMD structures in comparison with canonical those of A-DNA (-·-·-) and B-DNA (- - -).

The plots for selected intra-base pair parameters are shown in Figure 6B. These helical parameters are fairly similar for the six rMD structures, the most important variation being around the abasic site, at the C_5·G_{18} and C_7·G_{16} base pairs. Buckles appear to be in reasonable agreement with the standard B-DNA form. However, the most pronounced deviation is observed for the C_7 nucleotide. In addition, this and the value for C_5 are poorly defined, varying between 5.05° and −1.32° and −6.46° and −11.20°, respectively. All the base pairs exhibit rather large shear in the opposite direction, thus maximizing base pair stacking interactions. Propeller twists are negative for all base pairs and are similar or larger than for classical B-DNA, as observed for other oligonucleotides in solution. Base pair openings display fluctuations around the ideal value for all base pairs.

The plots for the selected inter-base pair parameters are shown in Figure 6C. Slide and base pair shifts differ little from those of standard structures (data not shown). Values for the rises are included between canonical A- and B-DNA forms, resulting in an overall length of the helix of 29.8 Å, which is 4 Å shorter than for standard B-DNA. Roll, twist, and tilt angles have values similar to those of standard structures.

DISCUSSION

Refined Structures. An assessment of the refined structures obtained from rMD calculations in terms of rmsd values, restraint violations, and *R* factors gives some perspective on the quality of the converged structures.

The calculated rmsd values between the two canonical A- and B-forms is 5.20 Å. While large rmsd values are observed between these two starting structures and the six rMD structures, mutual rmsd values between the rMD structures are much lower (∼1 Å). These data point out that good convergence has been achieved. This successful convergence

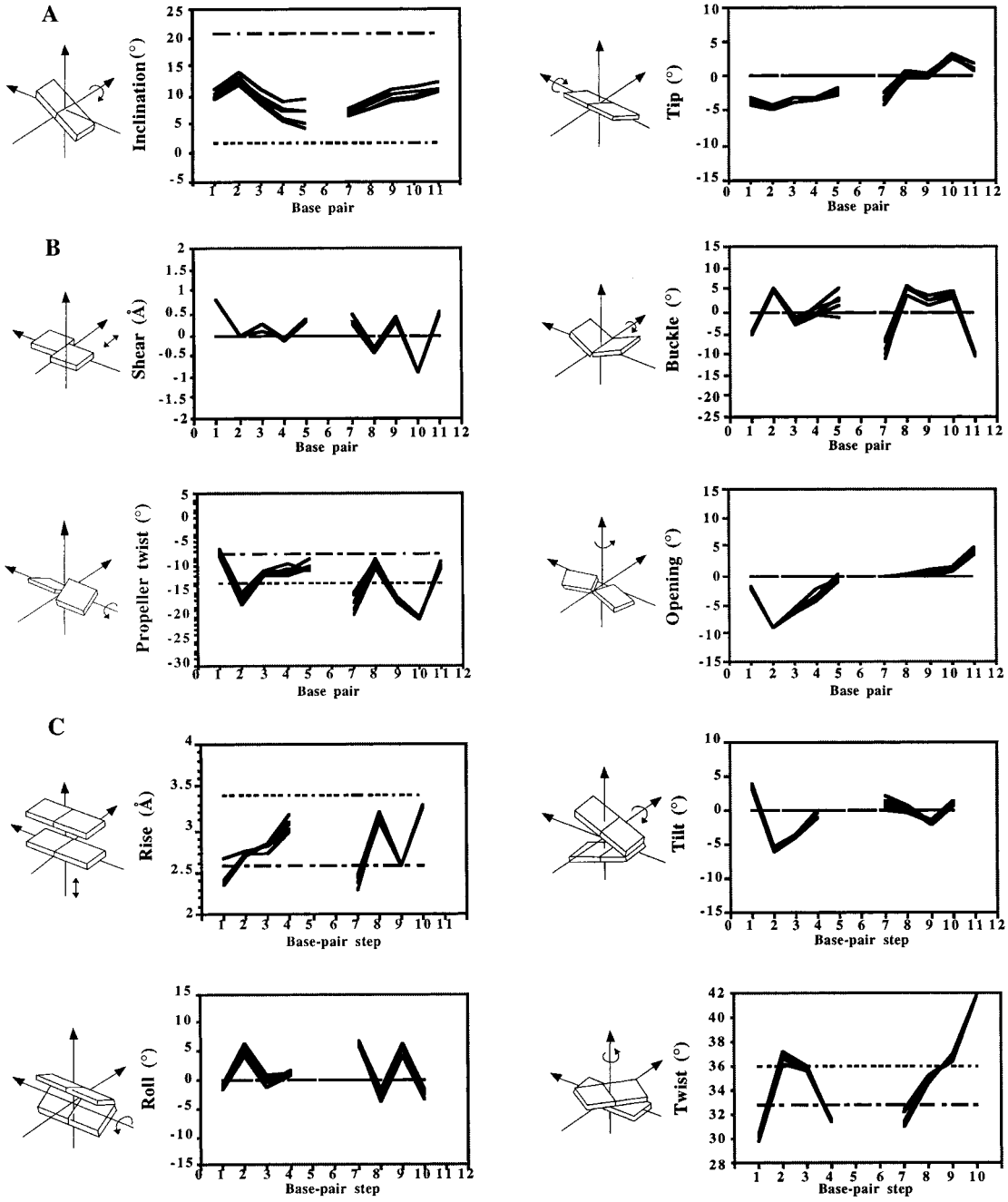

FIGURE 6: Helical parameters for the six refined structures compared to those of standard A-DNA (-·-·-) and B-DNA (- - -): axis−base pair parameters (A), intra-base pair parameters (B), and inter-base pair parameters (C).

to a similar conformation is indicative of the precision of the rMD calculations. Most significant differences arise at the terminal base pairs and can probably be attributed to end fraying.

As for rmsd values, constraint violations show large improvements for rMD structures relative to the initial ones. Among the 172 distance and 105 dihedral angles restraints, only five distance violations greater than 0.2 Å and four angle violations greater than 10° are found for the refined structures.

The accuracy of the refined structures has been judged by direct comparison between the experimental and back-calculated NOESY spectra. Thus, residual indices R^x and R^c have been used to evaluate the consistency of these structures with the experimental data. The refined structure was considered to be accurate as can be seen by the small values of the *R* factors when compared to those of the Ini-A and Ini-B structures (Table 2).

T17 Stacks Inside the Helix. The position of T_{17} in the duplex is well-defined since several NOE contacts are visible for this residue. The observed NOEs between the T_{17} sugar protons and the G_{18}-H8 proton, and between T_{17}-CH_3 and G_{16}-H8, indicate that T_{17} remains inside the helix. Moreover, the absence of a NOE between the imino protons of G_{16} and G_{18} is consistent with a stacked T_{17} residue in the abasic site pocket. Figure 7A represents the T_{17} nucleotide flanked by C_5·G_{18} and C_7·G_{16} base pairs, and shows that the refined structure agrees well with the NMR observations. Furthermore, the T_{17} backbone torsion angles, sugar pucker, and helical parameters (Figures 5 and 6) are similar to those in standard DNA forms, and no significant structural perturbation is observed for this residue.

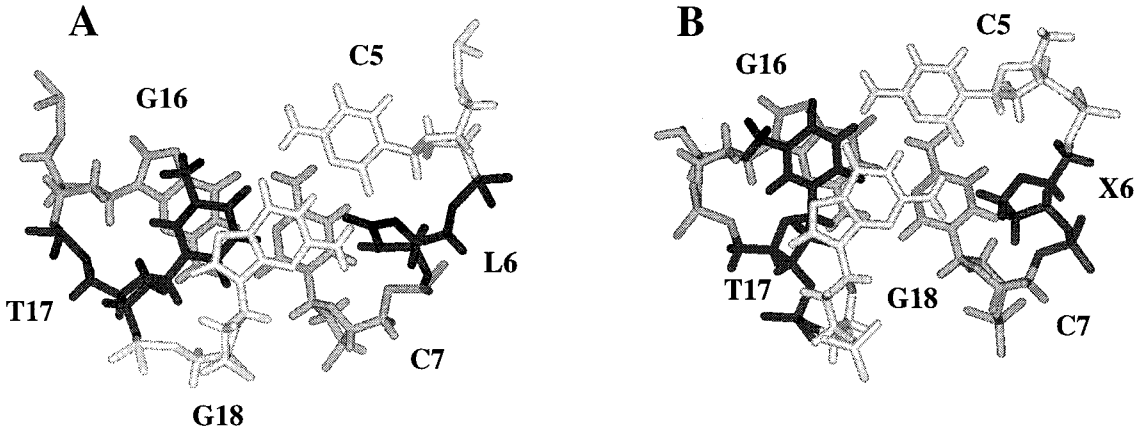

FIGURE 7: View looking down the helix axis of the central region of the duplexes containing the 2′-deoxyribonolactone (A) or 2′-deoxyribose analogue (B) damage sites. Note the good stacking of T_{17} between adjacent guanines and the position of the lactone ring (L_6) inside the helix in panel A.

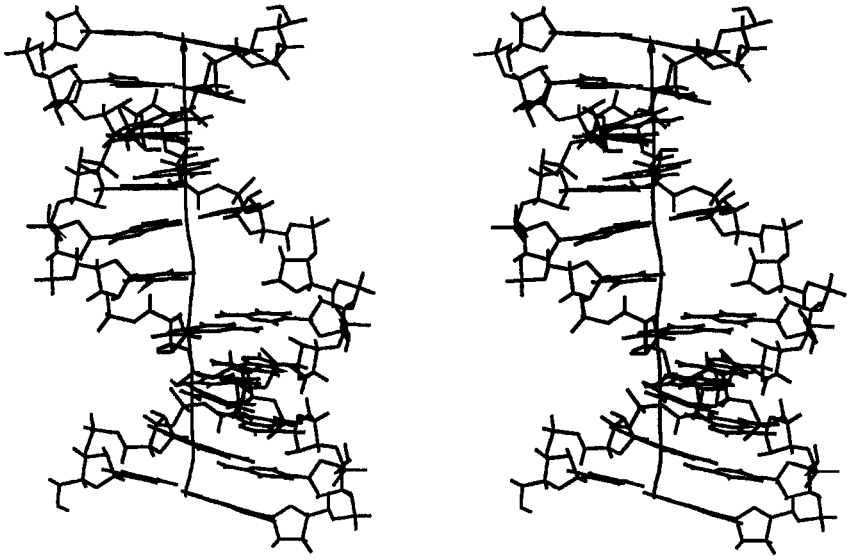

FIGURE 8: Stereoview of the average rMD structure (RS-ave) with its calculated global helix axis. This view is into the major groove.

Abasic Site L_6. The position of the lactone ring is not well-defined since very few distances involving this residue and the flanking bases could be calculated. We could observe NOE correlations between L_6-H2′/H2″ and C_7-H6, but with intensities weaker than expected for a regular structure (Figure 1). These data indicate that a structural perturbation arises at the abasic site, but reveal also an intrahelical position for the lactone ring. Moreover, close inspection of the lactone line width indicates that this residue is not involved in a dynamic process with an extrahelical position, even at a temperature of up to 30 °C.

Furthermore, the temperature dependence of the intensity and chemical shift of resonances of the imino protons displayed in Figure 2 indicates a shorter imino lifetime for G_{16} and perhaps G_{18} than for nonterminal base pairs. Thus, the presence of the abasic site induces a specific destabilization of the adjacent base pairs and particularly of C_7·G_{16}, at the 3′-side.

Sugar Puckers and Backbone Torsion Angles. Sugar puckers are well-defined by NMR restraints, and all rMD structures converge to quite similar geometries (Figure 5B). Glycosidic rings display pseudorotation angles *P* in the S range with conformations between C1′-exo and C2′-endo, except for terminal residues C_1 and G_{22}. Glycosidic angles χ are all in the anti domain.

Whereas direct NOE data are not available to restrain the position of the atoms in the phosphodiester backbone, good convergence is generally observed for all torsion angle values. This can probably be attributed to the right-handedness restraints used in the work described here. However, the force constant used (5 kcal mol^{-1} rad^{-2}) is weak enough to be compatible with other conformational features (*65*, *66*). Thus, the structure is essentially being defined by the experimental data. The most significant deviations are located around the abasic site and probably arise from a paucity of restraints at this step (vide supra).

Comparison with an Oligonucleotide Containing an AP Site. In a previous work, a stable tetrahydrofuran analogue of the 2′-deoxyribose site (X6 in ref *38*) was incorporated into a duplex possessing a sequence identical to that used in this study, and was examined in the same way (*38*). It is thus possible to perform a direct structural comparison between these two DNA lesions.

The exchangeable and nonexchangeable proton spectra are nearly similar for the two damaged duplexes. The only chemical shift differences greater than 0.1 ppm observed

between the two duplexes occur at the H5 (0.1 ppm) and sugar H1′ (−0.1 ppm) of residue C_7, when proceeding from the lactone to the AP site duplex. These chemical shift differences are relatively small and indicate that the base pairs flanking the damage sites assume similar conformations in the two duplexes. The shielding of T_{17}-CH_3 (−0.08 ppm) can suggest a slightly better stacking for this residue in the lactone than in the AP site duplex. The lactone ring and the tetrahydrofuran moiety differ in their NOE contacts with the C_7 nucleotide. Effectively, medium NOEs are detected between L_6-H2′/H2″ and C_7-H6 protons for the lactone site duplex, while these correlations were totally missing for the AP site duplex. This result indicates that the lactone ring is less shifted toward the minor groove than was the tetrahydrofuran moiety.

Identical behavior is also observed for the imino protons in the two undecamers when raising the temperature. Furthermore, the NOEs detected between exchangeable protons demonstrate that the two baseless sites are flanked by intact C_5·G_{18} and C_7·G_{16} Watson−Crick base pairs at low temperatures (10 °C). Finally, a destabilization of the C_7·G_{16} base pairs on the 3′-side of the abasic site is noticed for the two oligonucleotides.

The ^{31}P spectra of the two duplexes differ in the pattern of their downfield-shifted resonance. The lactone site duplex has only one resonance (i.e., C_{5p}-L_6) shifted downfield of the chemical range of unperturbed phosphodiester backbone resonances. On the other hand, the AP site duplex has two resonances deshielded, which were assigned to C_{5p}-X_6 and X_{6p}-C_7. These data indicate that the backbone may assume different conformations in the two duplexes at the abasic site step.

NMR results have been used to obtain refined structures for the two DNA duplexes. Figure 7 focuses on the central part of the two oligonucleotides and shows a good agreement between qualitative analysis of NMR features discussed above, and rMD structures. However, some differences are observed in the calculated conformations, notably, in the twist, tilt, and roll values for base pairs flanking the abasic sites. These differences result in kinking toward the major groove for the AP site duplex, which is not observed for the lactone site duplex.

CONCLUSION

As previously observed for the tetrahydrofuran abasic site, 2′-deoxyribonolactone in a DNA duplex induces little change in the general DNA structure that remains in the B-form with only localized perturbations at the site of the lesion. In the sequence context examined here, i.e., an apurinic lesion flanked by two cytosines, the thymine residue opposite the lesion adopts an intrahelical location as observed for the regular abasic site. However, common to the two types of modifications is the considerable destabilization of the duplexes as evidenced by the thermal denaturation experiments ($\Delta T_m \approx 20$ °C). Destabilization and flexibility at the damaged sites may represent the essential features in terms of recognition by repair enzymes, and this is consistent with the hypothesis that defects in DNA are located by repair enzymes due to lesion-induced alterations in duplex energetics (*67*). In relation to the structural observations presented here, it will be of great interest to elucidate recognition of 2′-deoxyribonolactone damage by polymerases and repair enzymes and compare the data to those reported for the regular 2′-deoxyribose abasic site. This work is now in progress, making use of the methodology developed for synthesizing DNA fragments containing the lactone lesion.

ACKNOWLEDGMENT

We thank Professor J. Reisse (Université Libre de Bruxelles, Brussels, Belgium) for fruitful discussions and for giving us access to the 600 MHz Varian spectrometer. We also thank C. Maerschalk for assistance with NMR spectroscopy and Miss V. Gineste for secretarial help.

SUPPORTING INFORMATION AVAILABLE

Three figures showing (1) the H1′−H2′/H2″ region of the DQF-COSY spectrum, (2) the H3′−H4′ region of the DQF-COSY spectrum, and (3) the imino to amino, H2 and H5 region of the 250 ms NOESY spectrum acquired in H_2O. This material is available free of charge via the Internet at http://pubs.acs.org.

REFERENCES

1. Pratviel, G., Bernadou, J., and Meunier, B. (1995) *Angew. Chem., Int. Ed. 34*, 746−769.
2. Pogozelski, W. K., and Tullius, T. D. (1998) *Chem. Rev. 98*, 1089−1107.
3. Naegeli, H. (1989) *Mechanisms of DNA damage recognition in mammalian cells*, pp 47−70, Springer-Verlag, Heidelberg, Germany.
4. Kappen, L. S., and Goldberg, I. H. (1989) *Biochemistry 28*, 1027−1032.
5. Pitié, M., Bernadou, J., and Meunier, B. (1995) *J. Am. Chem. Soc 117*, 2935−2936.
6. Pratviel, G., Bernadou, J., and Meunier, B. (1998) *Adv. Inorg. Chem. 45*, 251−312.
7. Decarroz, C., Wagner, J. R., and Cadet, J. (1987) *Free Radical Res. Commun. 2*, 295−301.
8. Von Sonntag, C., and Schuchmann, H. P. (1991) *Angew. Chem., Int. Ed. 30*, 1229−1253.
9. Urata, H., and Akagi, M. (1991) *Nucleic Acids Res. 19*, 1773−1778.
10. Goyne, T. E., and Sigman, D. S. (1987) *J. Am. Chem. Soc. 109*, 2846−2848.
11. Zelenko, O., Gallagher, J., Xu, Y., and Sigman, D. S. (1998) *Inorg. Chem. 37*, 2198−2204.
12. Meijler, M. M., Zelenko, O., and Sigman, D. S. (1997) *J. Am. Chem. Soc. 119*, 1135−1136.
13. Chen, T., and Greenberg, M. M. (1998) *J. Am. Chem. Soc. 120*, 3815−3816.
14. Bose, R. N., Fonkeng, B. S., Moghaddas, S., and Stroup, D. (1998) *Nucleic Acids Res. 26*, 1588−1596.
15. Sugiyama, H., Tsutsumi, Y., and Saito, I. (1990) *J. Am. Chem. Soc. 112*, 6720−6721.
16. Tronche, C., Goodman, B. K., and Greenberg, M. M. (1998) *Chem. Biol. 5*, 263−271.
17. Goldberg, I. H. (1991) *Acc. Chem. Res. 24*, 191−198.
18. Von Sonntag, C. (1987) *The Chemical Basis of Radiation Biology*, Taylor & Francis Inc., Philadelphia, PA.
19. Lindahl, T., and Nyberg, B. (1972) *Biochemistry 11*, 3610−3618.
20. Laval, E., and Laval, F. (1980) in *Enzymology of DNA Repair, in Molecular and Cellular Aspects of Carcinogen Screening Tests* (Montesano, R., Bach, H., and Tomatis, L., Eds.) Vol. 27, pp 55−73, IARC Scientific Publications, Lyon, France.
21. Lindahl, T. (1982) *Annu. Rev. Biochem. 51*, 61−87.
22. Weiss, B., and Grossman, L. *(1987) Adv. Enzymol. Relat. Areas Mol. Biol. 60*, 1−34.
23. Sancar, A., and Sancar, G. B. (1988) *Annu. Rev. Biochem. 57*, 29−67.

24. Myles, G. M., and Sancar, A. (1989) *Chem. Res. Toxicol. 2*, 197−226.
25. Povirk, L. F., Houlgrave, C. W., and Han, Y.-H. (1988) *J. Biol. Chem. 263*, 19263−19266.
26. Povirk, L. F., and Goldberg, I. H. (1985) *Proc. Natl. Acad. Sci. U.S.A. 82*, 3182−3186.
27. Kappen, L. S., Chen, C.-Q., and Goldberg, I. H. (1988) *Biochemistry 27*, 4331−4340.
28. Häring, M., Rüdiger, H., Demple, B., Boiteux, S., and Epe, B. (1994) *Nucleic Acids Res. 22*, 2010−2015.
29. Withka, J. M., Wilde, J. A., and Bolton, P. H. (1991) *Biochemistry 30*, 9931−9940.
30. Singh, M. P., Hill, G. C., Péoc'h, D., Rayner, B., Imbach, J.-L., and Lown, J. W. (1994) *Biochemistry 33*, 10271−10285.
31. Goljer, I., Kumar, S., and Bolton, P. H. (1995) *J. Biol. Chem. 270*, 22980−22987.
32. Wang, K. Y., Parker, S. A., Goljer, I., and Bolton, P. H. (1997) *Biochemistry 36*, 11629−11639.
33. Takeshita, M., Chang, C. N., Johnson, F., Will, S., and Grollman, A. P. (1987) *J. Biol. Chem. 262*, 10171−10179.
34. Cuniasse, Ph., Sowers, L. C., Eritja, R., Kaplan, B., Goodman, M. F., Cognet, J. A. H., Lebret, M., Guschlbauer, W., and Fazakerley, G. V. (1987) *Nucleic Acids Res. 15*, 8003−8022.
35. Cuniasse, Ph., Fazakerley, G. V., Guschlbauer, W., Kaplan, B. E., and Sowers, L. C. (1990) *J. Mol. Biol. 213*, 303−314.
36. Kalnick, M. W., Chang, C. N., Grollman, A. P., and Patel, D. J. (1988) *Biochemistry 27*, 924−931.
37. Kalnick, M. W., Chang, C. N., Johnson, F., Grollman, A. P., and Patel, D. J. (1989) *Biochemistry 28*, 3373−3383.
38. Coppel, Y., Berthet, N., Coulombeau, C., Coulombeau, Ce., Garcia, J., and Lhomme, J. (1997) *Biochemistry 36*, 4817−4830.
39. Kotera, M., Bourdat, A.-G., Defrancq, E., and Lhomme, J. (1998) *J. Am. Chem. Soc. 120*, 11810−11811.
40. Freeman, R., Friedrich, J., and Xi-Li, W. (1988) *J. Magn. Reson. 79*, 561−567.
41. Plateau, P., and Gueron, M. (1982) *J. Am. Chem. Soc. 104*, 7310−7311.
42. Hosur, R. V., Ravikumar, M., Chary, K. V. R., Shteth, A., Govil, G., Zun-Kun, T., and Miles, H. T. (1986) *FEBS Lett. 205*, 71−76.
43. Altona, C., and Sundaralingam, M. (1972) *J. Am. Chem. Soc. 94*, 8205−8211.
44. Borgias, B. A., and James, T. L. (1989) *Methods Enzymol. 176*, 169−183.
45. Borgias, B. A., and James, T. L. (1990) *J. Magn. Reson. 87*, 475−487.
46. Liu, H., Thomas, P. D., and James, T. L. (1992) *J. Magn. Reson. 98*, 163−175.
47. Arnott, S., Chandrasekaran, R., Birdsall, D. L., Leslie, A. G. W., and Ratliff, R. L. (1980) *Nature 283*, 743−745.
48. Reid, B. R., Banks, K., Flynn, P., and Nerdal, W. (1989) *Biochemistry 28*, 10001−10007.
49. Biosym/MSI (1997) *Insight II 97.0/Discover 97.0*, 9685 Strandon Rd., San Diego, CA.
50. Weiner, S. J., Kollman, P. A., Nguyen, D. T., and Case, D. A. (1986) *J. Comput. Chem. 7*, 230−252.
51. Saenger, W. (1984) *Principles of Nucleic Acid Structure*, Springer-Verlag, New York.
52. Baleja, J. D., Pon, R. T., and Sykes, B. D. (1990) *Biochemistry 29*, 4828−4839.
53. Metzler, W. J., Wang, C., Kitchen, D. B., Levy, R. M., and Pardi, A. (1990) *J. Mol. Biol. 214*, 711−736.
54. Wang, Y., and Patel, D. J. (1994) *J. Mol. Biol. 242*, 508−526.
55. Keepers, J. W., and James, T. L. (1984) *J. Magn. Reson. 57*, 404−426.
56. Borgias, B. A., and James, T. L. (1988) *J. Magn. Reson. 79*, 493−512.
57. James, T. L. (1991) *Curr. Opin. Struct. Biol. 1*, 1042−1053.
58. Lavery, R., and Sklenar, H. (1996) *Curves 5.1 Manual*, CNRS, Paris.
59. Lavery, R., and Sklenar, H. (1988) *J. Biomol. Struct. Dyn. 6*, 63−91.
60. Lavery, R., and Sklenar, H. (1989) *J. Biomol. Struct. Dyn. 6*, 655−667.
61. Hare, D. R., Wemmer, D. E., Chou, S.-H., Drobny, G., and Reid, B. R. (1983) *J. Mol. Biol. 171*, 319−336.
62. Wüthrich, K. (1986) *NMR of Proteins and Nucleic Acids*, pp 203−255, John Wiley & Sons, New York.
63. Scheek, R. M., Russo, N., Boelens, R., Kaptein, R., and Van Boom, J. H. (1983) *J. Am. Chem. Soc. 105*, 2914−2916.
64. Gorenstein, D. G. (1994) *Chem. Rev. 94*, 1315−1338.
65. Schmitz, U., Sethson, I., Egan, W., and James, T. L. (1992) *J. Mol. Biol. 227*, 510−531.
66. Mujeeb, A., Kerwin, S. M., Kenyon, G. L., and James, T. L. (1993) *Biochemistry 32*, 13419−13431.
67. Gelfand, C. A., Plum, E., Grollman, A. P., Johnson, F., and Breslauer, K. J. (1998) *Biochemistry 37*, 7321−7327.

BI982743R